Letters

A Maximum-Power-Point Tracking Method Based on Constant Conduction Time Control With Constant Voltage Output for Magnetic Field Energy Harvesters in the Saturated Region

Zhaowei Liu, Yong Li, *Senior Member, IEEE*, Xianglin Wen, Ziqian Hu, Huanyu Yang, and Zhengyou He, *Senior Member, IEEE*

***Abstract*—To improve the power density of magnetic field energy harvesters (MFEHs) and supply stable voltage output, a maximum-power-point tracking (MPPT) method with constant voltage (CV) output for the MFEH in the saturated region is proposed. The proposed MFEH system consists of a bidirectional buck–boost converter connected with a supercapacitor and an active rectifier. The bidirectional buck–boost converter is employed for CV output control, and MPPT under CV output conditions is realized by controlling the conduction time of the active rectifier. Besides, the calculation formula for the optimal conduction time in the saturated region is derived, which is constant and does not vary with the primary current. Subsequently, the optimal coil turn design method of the MFEH under optimal conduction time control is proposed, which can be used to guide the design of the coil turns. An experimental prototype is constructed to verify the effectiveness of the proposal. Experimental results demonstrate that the output voltage can be maintained at 3.3 V, and CV output can be realized. Besides, compared to conventional methods, the output power of the MFEH with the proposed method at 50 A_{rms} increases from 0.47 to 0.60 W, achieving a 27% improvement.**

***Index Terms*—Constant voltage (CV) output, magnetic field energy harvesters (MFEHs), maximum-power-point tracking (MPPT), optimal conduction time.**

I. Introduction

IN RECENT years, there has been significant interest in emerging technologies in power systems, such as the smart grid (SG) and the ubiquitous power Internet of Things [1]. Online monitoring devices play a crucial role in achieving system intelligence by monitoring and reporting the status of transmission lines, including current, voltage, humidity, and temperature. The increasing deployment of these devices in the SG has created a high demand for power sources [2].

As the most common power supply method, batteries have the drawback of requiring frequent charging and replacement. Currently, energy harvesting (EH) techniques offer a promising solution for powering wireless sensing and online monitoring devices. Over the past decade, extensive research has been conducted on EH techniques for various sources, such as solar, wind, vibration, radio frequency, and magnetic field. Solar energy harvesters and wind energy harvesters are relatively mature, but they are susceptible to weather conditions, which limits their applications. Vibration energy harvesters and radio frequency energy harvesters are less affected by weather conditions but have extremely low power densities.

The magnetic field energy harvesters (MFEHs) generate electrical energy directly by extracting energy from the magnetic field surrounding the transmission lines. Due to its weather-independent nature and relatively high power density, the MFEH is considered a suitable EH method near transmission lines.

Ensuring the normal operation of the online monitoring devices requires stable voltage and sufficient power. Recently, the power demand for online monitoring equipment has increased. Especially, industrial robots and drone charging stations require enormous power. Besides, the power supply equipment in the transmission line environment has strict restrictions on volume and weight. To meet the power supply requirements of the online monitoring equipment within limited volume and weight constraints, the maximum-power-point tracking (MPPT) method of MFEH has been extensively studied [3], [4], [5].

Liu et al. [3] propose a power-boosting method based on series-connected capacitors, which effectively enhances the harvesting power. A control strategy of MFEH based on impedance matching theory is proposed in [4], which can track the maximum power under varying currents. A power-improving method based on transfer window alignment is proposed in [5], leading to significant improvements in harvesting power. These methods can improve the harvesting power, but the output voltage regulation is sacrificed.

Manuscript received 3 April 2024; revised 13 May 2024; accepted 13 June 2024. Date of publication 19 June 2024; date of current version 16 July 2024. This work was supported in part by the Natural Science Foundation of Sichuan Province under Grant 2024NSFJQ0011, in part by the Cutting-Edge Science and Technology Cultivation Project of Southwest Jiaotong University under Grant 2682022KJ005, and in part by the Fundamental Research Funds for the Central Universities under Grant 2682023ZTPV026. *(Corresponding author: Yong Li.)*

The authors are with the School of Electrical Engineering, Southwest Jiaotong University, Chengdu 610031, China (e-mail: liuzw@my.swjtu.edu.cn; yong_li@swjtu.edu.cn; m18188331008@my.swjtu.edu.cn; huzq@my.swjtu.edu.cn; yanghy@my.swjtu.edu.cn; hezy@swjtu.edu.cn).

Color versions of one or more figures in this article are available at https://doi.org/10.1109/TPEL.2024.3416456.

Digital Object Identifier 10.1109/TPEL.2024.3416456

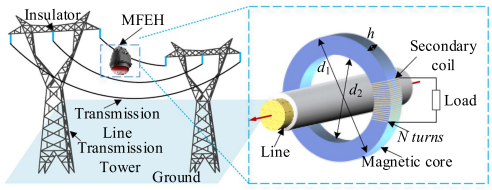

Fig. 1. Fundamental concept and structure of the MFEH installed in transmission lines.

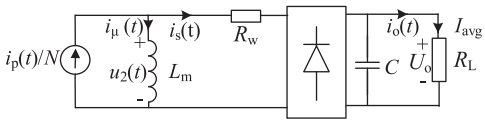

Fig. 2. Equivalent circuit of the MFEH with a diode rectifier.

An energy management method is proposed using bidirectional dc–dc converters in conjunction with a supercapacitor (SC) in [6]. By using this method, constant voltage (CV) output can be realized, and the MFEH is controlled to operate at the maximum power point in the unsaturated region. As detailed in [7] and [8], although the average output current decreases when the magnetic core enters the saturated region, the output voltage increases, so controlled saturation is critical to increasing the harvesting power of the MFEH. Therefore, to further improve the power density of MFEHs and supply stable voltage output, achieving both MPPT and CV output simultaneously for the MFEH in the saturated region has become an urgent mission.

To fill the above research gap, an MPPT method with CV output for the MFEH in the saturated region is proposed in this work. The main contributions are summarized as follows.

1) In this work, the calculation formula for the optimal conduction time of the active rectifier is derived to realize MPPT under CV output conditions. It is demonstrated that for a given MFEH, the optimal conduction time of the active rectifier remains constant, regardless of the variations in primary current. Based on a bidirectional buck–boost converter connected with an SC and an active rectifier, MPPT and CV output can be realized simultaneously by controlling the conduction time.
2) Under optimal conduction time control, changing the coil turns can affect the harvesting power. An optimal coil turn design method is presented in this work, which can be used to guide the design of the coil turns.

II. Theoretical Analysis

A. System Configuration

The fundamental concept of the MFEH installed in transmission lines is illustrated in Fig. 1. N is the number of coil turns, d_1 is the outer diameter of the core, d_2 is the inner diameter of the core, and h is the height of the core.

The primary side current $i_{\mathrm{p}}(t)$, i.e., the current of the transmission line, is a sinusoidal wave with a period of T, which can be expressed as

$$i_{\mathrm{p}}(t) = \sqrt{2} I_{\mathrm{p}} \sin(2\pi t/T) = \sqrt{2} I_{\mathrm{p}} \sin(\omega t) \tag{1}$$

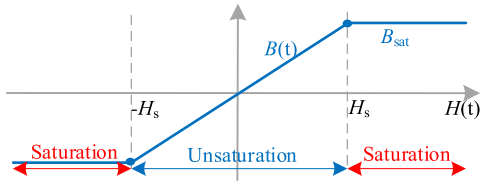

Fig. 3. Idealized B–H curve.

where I_{p} is the root-mean-square (rms) value of the primary side current, and ω is the angular frequency.

B. Equivalent Circuit of the MFEH

Fig. 2 shows the equivalent circuit of the MFEH with a diode rectifier. L_{m} is the magnetizing inductance, R_{w} is the internal resistance of the coil, $i_{\mathrm{s}}(t)$ is the secondary-side current, $i_{\mu}(t)$ is the magnetizing current, $i_{\mathrm{o}}(t)$ is the output current, C is the filter capacitor, R_{L} is the resistance of load, $u_2(t)$ is the voltage across the secondary side, and U_{o} is the voltage across R_{L}.

Due to the high permeability and ignorable hysteresis loss of the permalloy core used in this work, the B–H curve of the magnetic core can be idealized, as shown in Fig. 3. The magnetic flux density of the core can be expressed as follows [6], [9]:

$$B = \begin{cases} \mu_0 \mu_{\mathrm{r}} H, & (\text{Unsaturation}) \\ \pm B_{\mathrm{sat}}, & (\text{Saturation}) \end{cases} \tag{2}$$

where μ_0 is the vacuum permeability, μ_{r} is the relative permeability, and B_{sat} is the saturation magnetic flux density of core material.

From (2) and Fig. 3, it can be seen that when the magnetic flux density has not reached $\pm B_{\mathrm{sat}}$, the magnetic core is unsaturated [9], [10]. When the flux reaches $\pm B_{\mathrm{sat}}$, the magnetic core is saturated. If the magnetic core does not saturate during operation, the MFEH operates in the unsaturated region. If the magnetic core periodically goes in and out of the saturated state during operation, the MFEH operates in the saturated region.

By applying Kirchhoff's current law, the following equation can be obtained:

$$i_{\mathrm{p}}(t)/N = i_{\mu}(t) + i_{\mathrm{s}}(t). \tag{3}$$

When the MFEH is unsaturated, since the equivalent impedance of L_{m} is much greater than the impedance of the load, the magnetizing current $i_{\mu}(t)$ can be neglected. When the MFEH is saturated, since L_{m} is reduced to almost zero, $i_{\mathrm{s}}(t)$ can be seen as zero. In this case, $i_{\mathrm{s}}(t)$ can be expressed as

$$i_{\mathrm{s}}(t) = \begin{cases} i_{\mathrm{p}}(t)/N, & (\text{Unsaturation}) \\ 0, & (\text{Saturation}). \end{cases} \tag{4}$$

By applying Kirchhoff's voltage law, the following equation can be obtained [6]:

$$U_2 = U_{\mathrm{o}} + 2U_{\mathrm{d}} + \bar{U}_{\mathrm{w}} \tag{5}$$

where U_2 is the amplitude of $u_2(t)$, U_{d} is the voltage of the diode, and $\bar{U}_{\mathrm{w}}$ is the average voltage across R_{w} in half a cycle. Since R_{w} is much smaller than the load resistance, R_{w} and $\bar{U}_{\mathrm{w}}$ can be neglected [6]. Therefore, (5) can be expressed as

$$U_2 = U_{\mathrm{o}} + 2U_{\mathrm{d}}. \tag{6}$$

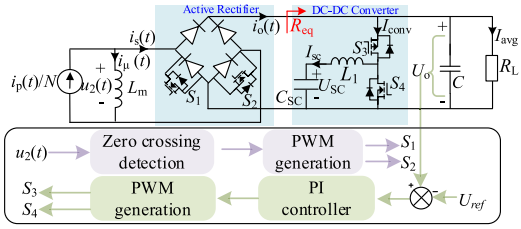

Fig. 4. Circuit diagram of the MFEH with a bidirectional buck–boost converter and an active rectifier.

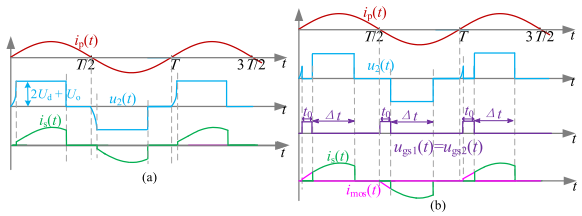

Fig. 5. Waveforms of $i_p(t)$, $u_2(t)$, $u_{gs1}(t)$, $u_{gs2}(t)$, $i_s(t)$, and $i_{mos}(t)$. (a) Conduction time control is not employed. (b) Conduction time control is employed.

III. MPPT Method With CV Output

A. CV Control Based on the Bidirectional Buck–Boost Converter

The bidirectional buck–boost converter composed of L_1, S_3, and S_4 is employed for regulating the output voltage. The bidirectional buck–boost converter links R_L and the SC, as shown in Fig. 4. S_3 and S_4 are controlled to turn ON alternately with a certain deadband.

As detailed in [6], by controlling the duty cycle of the bidirectional buck–boost converter, CV output can be realized, during which the SC undergoes adaptive charging and discharging. When the current is high and the power harvested by the MFEH exceeds the power consumed by the load, the current flows into the SC. When the current is low and the power harvested by the MFEH is insufficient to support the load consumption, the current flows out of the SC. In this process, the following equations can be obtained:

$$D = U_{SC}/U_o = I_{conv}/I_{SC} \tag{7}$$

where D is the duty cycle of the buck–boost converter, I_{conv} is the current flowing into the converter, U_{SC} is the voltage of the SC, and I_{SC} is the current flowing into the SC.

B. Numerical Solution for the Optimal Conduction Time

Two actively controlled MOSFETs (S_1, S_2) are connected to the diode rectifier, as shown in Fig. 4. Due to the low ON-resistance of the MOSFET, typically in the milliohm range, when S_1 and S_2 are turned ON simultaneously, the current flowing through the MOSFETs, i.e., $i_{mos}(t)$, is much greater than $i_s(t)$, and $i_s(t)$ can be seen as zero. When S_1 and S_2 are turned OFF simultaneously, $i_{mos}(t)$ is equal to zero.

When conduction time control is not employed, in the saturation region, the waveforms of $i_p(t)$, $u_2(t)$, and $i_s(t)$ are shown in Fig. 5(a). When the magnetic core is saturated, the permeability decreases, causing $u_2(t)$ to drop to zero [8]. After $i_p(t)$ passes through the zero-crossing point, the magnetic core begins to magnetize, and $u_2(t)$ rises from zero to $2U_d + U_o$ [1].

When conduction time control is employed, the waveforms of $i_p(t)$, $u_2(t)$, $u_{gs1}(t)$, $u_{gs2}(t)$, $i_s(t)$, and $i_{mos}(t)$ are shown in Fig. 5(b). t_0 is the conduction time of S_1 and S_2 starting from the zero-crossing point of $i_p(t)$, and Δt is the EH time in each half-cycle. $u_{gs1}(t)$ and $u_{gs2}(t)$ are the gate control signals of S_1 and S_2, respectively. It is difficult to collect $i_p(t)$, and without any control, the zero-crossing point of $u_2(t)$ is almost synchronized with $i_p(t)$. Thus, the controller senses the zero-crossing point of $u_2(t)$ as a reference to generate $u_{gs1}(t)$ and $u_{gs2}(t)$. When the controller detects that $u_2(t)$ exceeds a certain value, it generates $u_{gs1}(t)$ and $u_{gs2}(t)$ to control the conduction of S_1 and S_2. Due to the low ON-resistance of the MOSFETs, $u_2(t)$ is pulled down. Thus, the peak of $u_2(t)$ is caused by the conduction of S_1 and S_2 in the active rectifier. The presence of the voltage peak of $u_2(t)$ results in accumulated magnetic flux, consequently leading to a shortened Δt. However, due to the relatively low amplitude and short duration of the voltage spikes, the accumulated magnetic flux during the voltage spike process constitutes a small proportion of the total magnetic flux. Therefore, in the process of analyzing the harvesting power of the MFEH, the voltage peak of $u_2(t)$ is ignored for ease of calculation.

According to [6], the maximum power point of the MFEH in the unsaturated region is the critical saturated point. In this case, the critical saturation voltage of the core, i.e., U_{2c}, can be expressed as

$$U_{2c} = 4NA_{core}B_{sat}/T \tag{8}$$

where A_{core} is the cross-sectional area of the core.

When U_2 exceeds U_{2c}, the magnetic core enters the saturated region, and Δt is less than $T/2$. The analysis of the maximum power in the saturated region is as follows.

The output power of MFEH can be expressed as

$$P_o = U_o\bar{I}_s \tag{9}$$

where $\bar{I}_s$ is the average of $i_s(t)$ in half a cycle.

Since U_o is controlled to remain constant, P_o is determined by $\bar{I}_s$. It is necessary to find the optimal t_0, i.e., t_{0opt}, to maximize $\bar{I}_s$, thereby achieving MPPT. In the saturated region, $\bar{I}_s$ can be expressed as

$$\bar{I}_s = \frac{2}{T}\frac{I_p}{N}\int_{t_0}^{t_0+\Delta t}\sin(\omega t)\,dt = \frac{2I_p}{TN}\left[\cos\omega t_0 - \cos\omega(t_0+\Delta t)\right]. \tag{10}$$

By differentiating $\bar{I}_s$ with respect to t_0 and setting it to zero, t_{0opt} can be gained by solving the following equation:

$$\frac{\partial\bar{I}_s}{\partial t_0} = \frac{2\omega I_p}{TN}\left[\sin\omega(t_0+\Delta t) - \sin\omega t_0\right] = 0. \tag{11}$$

By solving (11), the following results can be obtained:

$$t_{0opt} = T/4 - \Delta t/2. \tag{12}$$

As detailed in [6], in the saturated region, U_2 can be expressed as

$$U_2 = 2B_{sat}A_{core}N/\Delta t. \tag{13}$$

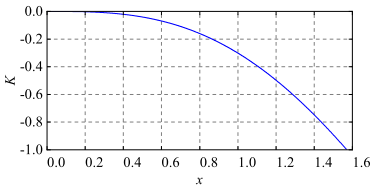

Fig. 6. K versus x.

Substituting (6) and (13) into (12), $t_{0\mathrm{opt}}$ can be derived as

$$t_{0\mathrm{opt}} = T/4 - B_{\mathrm{sat}}A_{\mathrm{core}}N/(U_{\mathrm{o}} + 2U_{\mathrm{d}}). \tag{14}$$

According to (14), $t_{0\mathrm{opt}}$ is related to B_{sat}, A_{core}, N, U_{d}, and U_{o}. Since U_{o} is controlled to be constant, for a given MFEH with fixed magnetic core and coil turns, $t_{0\mathrm{opt}}$ remains constant. This means that for a given MFEH, the optimal t_0 for achieving MPPT is constant, regardless of variations in primary current.

C. Design of Optimal Coil Turns

Substituting (10) and (12) into (9), the following expression can be obtained:

$$P_{\mathrm{o}} = 2U_{\mathrm{o}}I_{\mathrm{p}}\sin(\omega\Delta t/2)/N\pi. \tag{15}$$

Substituting (6) and (13) into (15), the following expression can be obtained:

$$P_{\mathrm{o}} = \frac{2U_{\mathrm{o}}I_{\mathrm{p}}}{N\pi}\sin\left(\frac{\omega B_{\mathrm{sat}}A_{\mathrm{core}}N}{U_{\mathrm{o}} + 2U_{\mathrm{d}}}\right). \tag{16}$$

According to (16), for a given magnetic core, varying U_{o} and N can affect P_{o} under optimal conduction time control. U_{o} is determined by the online monitoring devices, while N is adjustable. To investigate the influence of N on P_{o} under constant U_{o}, the derivative of P_{o} with respect to N is as follows:

$$\frac{\partial P_{\mathrm{o}}}{\partial N} = \frac{2U_{\mathrm{o}}I_{\mathrm{p}}}{N^2\pi}\left[\frac{B_{\mathrm{sat}}A_{\mathrm{core}}N\omega}{U_{\mathrm{o}} + 2U_{\mathrm{d}}}\cos\left(\frac{B_{\mathrm{sat}}A_{\mathrm{core}}N\omega}{U_{\mathrm{o}} + 2U_{\mathrm{d}}}\right) - \sin\left(\frac{B_{\mathrm{sat}}A_{\mathrm{core}}N\omega}{U_{\mathrm{o}} + 2U_{\mathrm{d}}}\right)\right]. \tag{17}$$

To find the critical points of P_{o}, the part within parentheses in (17) can be represented as

$$K = x\cos(x) - \sin(x) \tag{18}$$

where x is expressed as

$$x = B_{\mathrm{sat}}A_{\mathrm{core}}N\omega/(U_{\mathrm{o}} + 2U_{\mathrm{d}}) = \omega\Delta t/2. \tag{19}$$

Since $0 < \Delta t < T/2$, the range of x is as follows:

$$x \in \{0, \pi/2\}. \tag{20}$$

K as a function of x is plotted in Fig. 6. It is shown that as N increases, x increases, and K remains less than 0. Thus, reducing N can improve the maximum power of the MFEH under optimal conduction time control. However, N cannot be reduced without limits. The design of N also needs to consider its impact on L_{m}. As detailed in [8], L_{m} can be expressed as

$$L_{\mathrm{m}} = N^2\mu_0\mu_{\mathrm{r}}h\ln(d_1/d_2)/(2\pi). \tag{21}$$

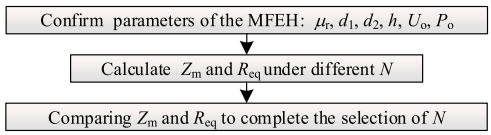

Fig. 7. Optimal turn design process.

TABLE I
Z_{M} UNDER DIFFERENT N

N	100	150	200	250	300
$Z_{\mathrm{m}}(\Omega)$	194.9	438.5	779.5	1218.0	1753.9

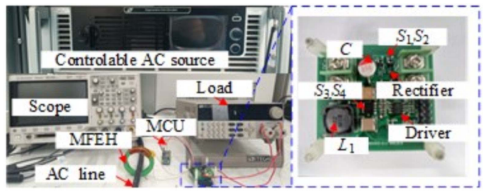

Fig. 8. Photograph of the experimental platform.

According to (21), reducing N will cause L_{m} to decrease rapidly, thereby increasing $i_\mu(t)$. If N is too small, $i_\mu(t)$ cannot be neglected, and (3) no longer holds. To ensure the validity of (3), when designing N, it is necessary to ensure that $Z_{\mathrm{m}} = \omega L_{\mathrm{m}}$, i.e., the impedance of L_{m} is much larger than the equivalent resistance of the load, i.e., R_{eq}, which can be expressed as

$$R_{\mathrm{eq}} = U_{\mathrm{o}}^2/P_{\mathrm{o}}. \tag{22}$$

The process of the optimal turn design method is shown in Fig. 7, and the key point of the optimal turn design method is to reduce N while ensuring that Z_{m} is significantly greater than R_{eq} (approximately 20 times).

Taking 3.3 V and 0.6 W as an example, $R_{\mathrm{eq}} = 3.3 \times 3.3/0.6\ \Omega = 18.15\ \Omega$. In China, the frequency of the transmission line is 50 Hz. A magnetic core with $d_1 = 75$ mm, $d_2 = 55$ mm, $h = 10$ mm, and $\mu_{\mathrm{r}} = 100\,000$ is used, and Z_{m} under different N are listed in Table I. When N reaches 100, Z_{m} reaches ten times of R_{DC}, but there will still be some current flowing into L_{m}. When N reaches 150, Z_{m} is more than 20 times greater than R_{DC}. Therefore, in this work, considering increasing harvesting power while reducing $i_\mu(t)$, N is chosen to be 150.

IV. Experimental Verifications

A. Experimental Setup

In this letter, an experimental platform is built in the laboratory for experimental verification, as shown in Fig. 8. In this process, a controllable ac source is connected to aluminum shell resistances to emulate an ac transmission line. Experiments are conducted to verify the effectiveness of the proposal. In this work, STM32F103C8T6 is employed as the controller. Permalloy 1j85 is selected as the core material, and $B_{\mathrm{sat}} = 0.58$ T. A magnetic core with $d_1 = 75$ mm, $d_2 = 55$ mm, and $h = 10$ mm is used. U_{d} of the diode employed is approximately 0.3 V. PMV30UN2R (S_1, S_2) and SM4862 (S_3, S_4) are employed as the MOSFETs. UCC37324 is employed as the driver.

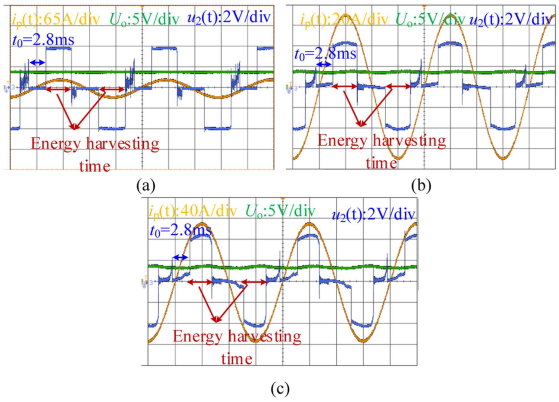

Fig. 9. Waveforms of $u_2(t)$, $i_p(t)$, and U_o with $N = 150$ under different I_p. (a) $I_p = 20\ A_{rms}$. (b) $I_p = 50\ A_{rms}$. (c) $I_p = 80\ A_{rms}$.

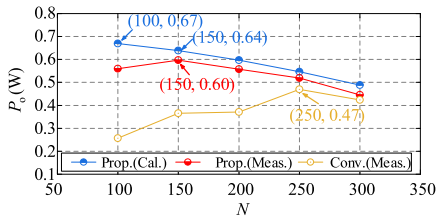

Fig. 10. Numerical calculations and measurement results of P_o according to N.

B. Verification of the MPPT Method With CV Output

Fig. 9 depicts the waveforms of $u_2(t)$, $i_p(t)$, and U_o with $N = 150$ under different I_p. It is shown that U_o remains at approximately 3.3 V. This means that the CV output is realized. Furthermore, it is shown in Fig. 9 that since the output voltage is controlled to be constant and Δt is constant, the optimal conduction time remains at 2.8 ms under different I_p. This simplifies the control procedure as there is no need for the controller to calculate the conduction time frequently.

As seen from Fig. 9, there exists a short-duration voltage peak of $u_2(t)$ before S_1 and S_2 are turned ON, which corresponds to the theoretical analysis in Section III-B. In addition, during t_0, $u_2(t)$ is not zero, and as $i_p(t)$ increases, the value of $u_2(t)$ gradually increases due to the presence of the internal resistance of the coil. During these two stages, $u_2(t)$ being nonzero will result in a slight accumulation of magnetic flux. Besides, due to the relatively low amplitude and short duration, the accumulated magnetic flux during these two stages constitutes a small proportion of the total magnetic flux. Thus, the impact of $u_2(t)$ being nonzero during these two stages on EH can be neglected. For the sake of simplified calculations, it is assumed in the theoretical derivation that $u_2(t)$ is approximately zero during these two stages, leading to the experimental values of the harvesting power being slightly lower than the calculated values, as shown in Fig. 10.

Fig. 10 shows the numerical calculations and measurement results of P_o according to N under $I_p = 50\ A_{rms}$. The numerical calculation results are obtained through (16). It can be observed that the measured power and calculated power of the proposed method are highly consistent, except for a difference at 100 turns. As analyzed in Section III, this discrepancy is caused by the small value of N, which results in the current shunting of L_m. When N exceeds 150, as N continues to increase, the harvesting power decreases, which is consistent with the analysis in Section III-C. This means that the optimal turn design method is valid.

In the conventional method proposed in [6], a passive rectifier is used for rectification, and a bidirectional buck–boost is used for CV control. Due to the lack of conduction time control, the maximum power at 50 A_{rms} is 0.47 W. In the proposed method, the maximum power of the MFEH at 50 A_{rms} is 0.60 W. Thus, compared to the conventional method, the output power of the MFEH with the proposed method significantly increases, with a maximum power improvement of 27%. Therefore, the method proposed in this letter can achieve MPPT and CV output simultaneously.

V. Conclusion

In this letter, an MPPT method with CV output for the MFEH in the saturated region is proposed. Coordinated control based on the bidirectional buck–boost converter and the active rectifier enables simultaneous implementation of MPPT and CV output. In addition, for fixed output voltage and MFEH parameters, the optimal conduction time remains constant, simplifying the control process. Experimental results demonstrate that the method proposed in this letter can achieve MPPT and CV output simultaneously, and the optimal turn design method is valid. Compared to the conventional method with a passive rectifier, the proposed method increases harvesting power by 27%.

References

[1] K. Ye et al., "A novel method of maximum power point reaching for magnetic field energy harvesting based on a low-power analog control circuit," *IEEE Trans. Power Electron.*, vol. 39, no. 1, pp. 1888–1897, Jan. 2024.

[2] A. Abramovitz, M. Shvartsas, and A. Kuperman, "Enhanced maximum power point reaching method for passive magnetic energy harvesters operating under low primary currents," *IEEE Trans. Power Electron.*, vol. 39, no. 6, pp. 6619–6623, Jun. 2024, doi: 10.1109/TPEL.2024.3376540.

[3] Z. Liu et al., "A novel method for magnetic energy harvesting based on capacitive energy storage and core saturation modulation," *IEEE Trans. Ind. Electron.*, vol. 70, no. 3, pp. 2586–2595, Mar. 2023.

[4] Y. Li, N. Duan, Z. Liu, J. Hu, and Z. He, "Impedance-matching based maximum power tracking for magnetic field energy harvesters using active rectifiers," *IEEE Trans. Ind. Electron.*, vol. 70, no. 10, pp. 10730–10739, Oct. 2023.

[5] J. Moon and S. B. Leeb, "Power electronic circuits for magnetic energy harvesters," *IEEE Trans. Power Electron.*, vol. 31, no. 1, pp. 270–279, Jan. 2016.

[6] Z. Liu, Y. Li, N. Duan, and Z. He, "An energy management method for magnetic field energy harvesters under wide-range current in railway electrification systems," *IEEE Trans. Ind. Electron.*, vol. 71, no. 5, pp. 5360–5369, May 2024.

[7] J. Moon and S. B. Leeb, "Analysis model for magnetic energy harvesters," *IEEE Trans. Power Electron.*, vol. 30, no. 8, pp. 4302–4311, Aug. 2015.

[8] Z. Liu, Y. Li, H. Yang, N. Duan, and Z. He, "An accurate model of magnetic energy harvester in the saturated region for harvesting maximum power: Analysis, design, and experimental verification," *IEEE Trans. Ind. Electron.*, vol. 70, no. 1, pp. 276–285, Jan. 2023.

[9] L. Du, C. Wang, X. Li, L. Yang, Y. Mi, and C. Sun, "A novel power supply of online monitoring systems for power transmission lines," *IEEE Trans. Ind. Electron.*, vol. 57, no. 8, pp. 2889–2895, Aug. 2010.

[10] M. Gao, L. Yi, and J. Moon, "Mathematical modeling and validation of saturating and clampable cascaded magnetics for magnetic energy harvesting," *IEEE Trans. Power Electron.*, vol. 38, no. 3, pp. 3455–3468, Mar. 2023.